



HAL
open science

Colloidal stability of capped silver nanoparticles in natural organic matter-containing electrolyte solutions

Leonardo Gutierrez, Andreas Schmid, Noor Zaouri, Daniel Garces,
Jean-Philippe Croué

► To cite this version:

Leonardo Gutierrez, Andreas Schmid, Noor Zaouri, Daniel Garces, Jean-Philippe Croué. Colloidal stability of capped silver nanoparticles in natural organic matter-containing electrolyte solutions. *NanoImpact*, 2020, 19, pp.100242 -. 10.1016/j.impact.2020.100242 . hal-03491631

HAL Id: hal-03491631

<https://hal.science/hal-03491631v1>

Submitted on 22 Aug 2022

HAL is a multi-disciplinary open access archive for the deposit and dissemination of scientific research documents, whether they are published or not. The documents may come from teaching and research institutions in France or abroad, or from public or private research centers.

L'archive ouverte pluridisciplinaire **HAL**, est destinée au dépôt et à la diffusion de documents scientifiques de niveau recherche, publiés ou non, émanant des établissements d'enseignement et de recherche français ou étrangers, des laboratoires publics ou privés.



Distributed under a Creative Commons Attribution - NonCommercial 4.0 International License

1

2 **Colloidal stability of capped silver nanoparticles in natural organic matter-**
3 **containing electrolyte solutions**

4

5

6

Submitted to

7

NanoImpact Journal

8

April 2020

9

10 Leonardo Gutierrez^{1,6*}, Andreas Schmid², Noor Zaouri³, Daniel Garces⁴, Jean-Philippe Croue^{5,*}

11

12

13

¹ Facultad del Mar y Medio Ambiente, Universidad del Pacifico, Ecuador

14 ² Department of Environmental Systems Science, Swiss Federal Institute of Technology ETH, Zurich, Switzerland

15 ³ Water Desalination and Reuse Center, King Abdullah University of Science and Technology, Saudi Arabia

16

⁴ Facultad de Ciencias de la Tierra, Escuela Superior Politecnica del Litoral

17

⁵ Institut de Chimie des Milieux et des Matériaux, IC2MP UMR 7285 CNRS, Université de Poitiers, France

18

⁶ Particle and Interfacial Technology Group, Department of Applied Analytical and Physical Chemistry, Ghent
19 University, Coupure Links 653, 9000, Ghent, Belgium

20

21 * Corresponding author: Tel.: +32 (0) 468358104

22 E-mail address: leo.gutierrez@upacifico.edu.ec

23 jean.philippe.croue@univ-poitiers.fr

24

25 28 pages, 6 figures, and a Supporting Information (SI) section are included in the current manuscript.

26 **Abstract**

27 Due to their increased production and commercial applications, capped silver nanoparticles
28 (AgNPs) have inevitably found their way into aquatic ecosystems. The mobility (fate/transport),
29 bioavailability, reactivity, and toxicity of capped AgNPs are highly influenced by their colloidal
30 stability. This study investigated the aggregation kinetics and interfacial interactions of tannic
31 acid (TA)-coated or silica-coated AgNPs in natural organic matter (NOM)-containing electrolyte
32 solutions by time-resolved dynamic light scattering and atomic force microscopy. Three well-
33 characterized NOM fractions of different characteristics were selected. In Na⁺-solutions, the
34 polymeric TA induced more stability to AgNPs than the hard silica coating. Although all NOM
35 fractions weakly interacted with TA even at high Na⁺ concentrations, these organics adsorbed on
36 the silica-coated AgNPs; thus, inducing stability. Humic fractions provided higher colloidal
37 stability due to stronger electrostatic/steric interactions. Ca²⁺ increased the aggregation kinetics
38 of both capped nanoparticles in the absence and presence of NOM. However, the aggregation
39 kinetics of TA-coated AgNPs in humic NOM-containing solution were higher than those of non-
40 humic due to a higher content of deprotonated carboxyl groups and cation bridging mechanisms.
41 The knowledge compiled in this study would assist in understanding and predicting the fate and
42 transport of capped nanoparticles in natural aquatic systems of different compositions.

43

44 **Keywords:** capped silver nanoparticles; natural organic matter; colloidal stability; aggregation;
45 dynamic light scattering.

46 **1. Introduction**

47 The production of engineered silver nanoparticles (AgNPs) in the industry has rapidly increased
48 due to their broad commercial applications (e.g., cosmetics, paints, food industry, medical fields,
49 and electronics) [1-3]. As a result, AgNPs have inevitably found their way into aquatic
50 ecosystems [4, 5]. The toxic impact of AgNPs would cause adverse effects on microbial
51 communities, aquatic organisms, and human health through possible chemical or physical
52 transformation reactions (i.e., sulfidation, dissolution, aggregation); thus, leading to changes in
53 crucial ecosystem processes [6, 7]. Remarkably, the bioavailability, reactivity, mobility, and
54 toxicity of manufactured AgNPs are highly influenced by their colloidal stability.

55 Colloidal stability in an aqueous solution is defined as the ability of particles to resist
56 aggregation over a specific time and is influenced by solution conditions (e.g., pH, ionic
57 strength-IS, electrolyte composition, and presence of natural organic matter-NOM) and type of
58 capping agents [8-10]. These capping agents (i.e., typically synthesized with different organic
59 surface coatings) are usually negatively charged species or long and hydrophilic polymers that
60 prevent aggregation of AgNPs by providing additional electrostatic, steric, or electrosteric
61 repulsive forces [11, 12]. Polyvinylpyrrolidone (PVP), polyethylene glycol (PEG), silica, tannic
62 acid (TA), and citrate are commonly used capping agents due to their high chemical stability,
63 low toxicity, and high solubility in polar solvents [12-18]. However, these capping agents would
64 interact with other water constituents (e.g., NOM, electrolytes), leading to changes in the
65 physicochemical properties of AgNPs surface (i.e., functionalities, surface charge,
66 hydrophobicity) [19, 20].

67 NOM and electrolytes are ubiquitous constituents in aquatic ecosystems that influence the fate
68 and transport of AgNPs [9, 21]. Previous studies have investigated the interactions between

69 NOM, electrolytes, and capped AgNPs using varied techniques, e.g., Time-Resolved Dynamic
70 Light Scattering (TR-DLS), Flow Field-Flow Fractionation, or Quartz Crystal Microbalance.
71 Briefly, bare AgNPs readily aggregate under low NaCl and CaCl₂ concentrations (i.e., critical
72 coagulation concentration-CCC: 40 and 2 mM, respectively), indicating their low stability in
73 solution [22]. Although capping agents prevent AgNPs from aggregating through steric
74 hindrance or additional electrostatic repulsion, the presence of high electrolyte concentrations or
75 divalent cations can lead to colloidal instability by charge screening or cation bridging,
76 respectively [13, 23, 24]. For instance, the CCC of PVP-coated and citrate-coated AgNPs in
77 CaCl₂ solution were lower than that in NaCl solutions at similar IS [20, 24]. Other studies have
78 also observed enhanced aggregation of capped AgNPs in divalent cation solutions [12, 19].
79 However, NOM interactions with AgNPs would increase colloidal stability. PVP-coated and
80 citrate-coated AgNPs were stabler in humic acid (HA)-containing NaCl solutions, while Ca²⁺
81 cations induced enhanced aggregation [20, 24]. HA in solution hindered the deposition of these
82 capped AgNPs on silica surfaces, confirming their mobility in NOM solutions under
83 environmentally relevant conditions [13].

84 Remarkably, due to the: a) increased production of capped AgNPs, and b) their environmental
85 impacts on natural water systems, there are at present concerted efforts to synthesize non-toxic
86 “green” AgNPs. Tannic acid (TA, highly biocompatible compound) is being increasingly used as
87 a stabilizing agent [15, 18]. TA is a weak acid and polyphenolic compound (hydrolyzed tannin)
88 of antimutagenic, anticancer, and antioxidant properties [25, 26]. Similarly, silica (i.e., a
89 ubiquitous mineral on earth) is also widely used as a capping agent for AgNPs in electronics,
90 optics, and biochemistry fields [16, 17]. Unlike their counterparts (e.g., citrate-, PVP-, and PEG-
91 coated AgNPs), the colloidal stability of TA-coated and silica-coated AgNPs in NOM-containing

92 electrolyte solutions has not been studied. This new knowledge would assist in understanding
93 and predicting their fate and transport in natural aquatic systems.

94 This study investigated the interfacial interactions and aggregation behavior of TA-coated and
95 silica-coated AgNPs in the presence of NOM and under different solution conditions. TA and
96 silica capping agents were selected due to their increased production and commercial
97 applications, and greener approach. Three well-characterized NOM isolates of different
98 properties were selected: two river humic fractions from Gartempe River (France) and Colorado
99 River (USA), and a hydrophilic isolate from Ribou River (France). Specifically, i) the
100 interactions between NOM and the polymeric surface of TA-coated AgNPs or the hard surface of
101 silica-coated AgNPs (i.e., hard vs. polymeric coatings are compared for the first time), and ii) the
102 influence of solution conditions (type and concentration of cations) were investigated. TR-DLS
103 technique was used to investigate aggregation kinetics of the capped AgNPs in NOM-containing
104 electrolyte solutions. Because NOM changes the surface properties of the capping agents upon
105 adsorption, Atomic Force Microscopy (AFM) in contact mode was used to study the
106 contributions of van der Waals, electrostatics, and steric mechanisms of every NOM isolate
107 during interfacial interactions. These experimental conditions were carefully selected to mimic
108 real environmental scenarios. The knowledge compiled would assist in identifying research
109 directions to understand and predict the fate and transport of capped nanoparticles in natural
110 aquatic systems of different compositions.

111 **2. Materials and Methods**

112 *2.1. Nanoparticles samples, reagents, and solution chemistries*

113 Electrolyte solutions for NOM stock preparation, AFM, and TR-DLS experiments were prepared
114 with ultrapure water (resistivity of 18 M Ω ·cm, Millipore, USA) and analytical grade agents (i.e.,

115 NaCl, CaCl₂, NaOH, FeCl₃, NaNO₃), and subsequently filtered through a 0.22 μm membrane.
116 The iron oxide solution used for the layer-by-layer coating procedure of AFM colloidal probes
117 was prepared by increasing the pH of a 10 mM FeCl₃ solution to 7 by small additions of NaOH,
118 as described elsewhere [27, 28]. Spherical silica-coated AgNPs (TEM silver core diameter:
119 70±10 nm, and silica shell thickness: 20±5 nm) and spherical TA-coated AgNPs (TEM diameter:
120 100±9.4 nm) were obtained from NanoXact (Nano-Composix, USA). Both capped nanoparticles
121 stocks were subjected to a dialysis-filtration process in a 1 mM NaNO₃ solution to remove
122 colloidal TA and dissolved silica species, using an Amicon cell (Millipore, USA). After this
123 purification process, the final concentration of both stocks of nanoparticles was approximately
124 20 ppm. Additionally, the quality of the stocks of nanoparticles was monitored for the duration
125 of this investigation by hydrodynamic diameter and electrophoretic mobility measurements.

126 **2.2. Origin, characteristics, and NOM stock preparation**

127 The NOM isolates selected for this investigation were obtained from three different surface
128 waters: a) Gartempe-HPO: a hydrophobic (HPO) NOM fraction extracted from a black water of
129 high humic content (i.e., high specific ultraviolet absorbance-SUVA) from Gartempe River,
130 France, b) Colorado-HPO: an HPO isolate collected from Colorado River, USA (low humic
131 content water), and c) Ribou-HPI: a biopolymer/hydrophilic (HPI) fraction from Ribou River,
132 France (non-humic, low SUVA water). These three fractions were isolated following the
133 comprehensive protocol described elsewhere [29], and have been rigorously characterized and
134 described in previous investigations and summarized in the SI section [20, 27, 30, 31]. The NOM
135 stock solutions were prepared by dissolving a NOM fraction in 1 mM NaCl solution, stirred
136 overnight, and filtered through a 0.45 μm membrane. The monodispersion of the dissolved NOM

137 was evidenced by TR-DLS (Figure S1). The final concentration of the NOM stock was
138 approximately 100 mg C/L.

139 *2.3. Electrophoretic Mobility (EPM) of the Natural Organic Matter isolates*

140 The EPM of NOM samples was measured using a ZS ZEN3600 Zetasizer (Malvern, UK) and
141 following the protocol described elsewhere [32]. Briefly, silica particles (1.6 μm in diameter,
142 Polysciences, Warrington, PA) were coated with Gartempe-HPO, Colorado-HPO, or Ribou-HPI
143 by the layer-by-layer method and using positively-charged iron oxide as an intermediate layer
144 [27]. 1 mL clear disposable zeta cells (DTS1060C, Malvern, UK) were used to measure the EPM
145 of NOM-coated silica particles under: 1, 3, 10, 30, and 100 mM NaCl solutions, and 0.33, 1,
146 3.33, 10, and 33.3 mM CaCl_2 solutions at ambient pH. These solution conditions are respectively
147 equivalent in terms of Ionic Strength. A minimum of three measurements was collected for every
148 solution condition. EPM values were converted to zeta potential by the Smoluchowski equation
149 using Dispersion Technology Software (v5.10, Malvern, UK). The data sets obtained were
150 pooled and the average results, including standard deviation, were presented in this study.

151 *2.4. Interaction forces between NOM fractions and mica surface*

152 AFM was used to study the dominant interacting mechanisms (i.e., electrostatic, van der Waals,
153 or steric interactions) between NOM and mica surface as a function of solution conditions. Mica
154 was selected as a model surface due to its high electronegativity (i.e., highly negatively-charged
155 surface). Based on Coulomb's law, the electrostatic repulsive forces between NOM isolates and
156 mica surface (i.e., forces proportional to the product of their charges) would be clearly detected
157 in the force vs. distance profiles generated by the AFM at different ionic strengths (IS) [27].
158 Steric repulsive forces would also be detected and discriminated against long-ranged exponential
159 electrostatic forces [33]. These results would assist in: i) identifying and measuring the
160 electrostatic and steric repulsive forces generated by each NOM fraction as a function of their

161 physicochemical characteristics and solution condition, and thus, ii) understand the interactions
162 between NOM and capped AgNPs.

163 A Dimension FastScan AFM (Bruker, USA) with an Icon Head was used to measure interaction
164 forces during the approaching regime. A ~ 20 μm silica sphere glued on a silicon nitride
165 cantilever with a manufacturer-reported spring constant of 0.24 N/m (SNL, Bruker, USA) was
166 used as an AFM colloidal probe and will be termed as AFM probe for the rest of this
167 investigation. These sensitive AFM probes of low spring constant/stiffness were selected to
168 record small forces originated from considerably small deflections of the cantilever during
169 interactions with soft materials (e.g., organic matter structures). The calibration of the AFM
170 probes was conducted as follows. Briefly, the deflection sensitivity of the AFM probes was
171 measured in air conditions and using freshly-cleaved mica as a control substrate. The spring
172 constant (k) of the cantilevers was determined by the Thermal Tuning method, where deflection
173 (V) was converted to force (nN) in accordance with Hooke's law [34]. No significant deviation
174 from the specification of the manufacturer was observed. The NOM coating of the AFM probes
175 was conducted following the layer-by-layer protocol and using positively-charged iron oxide as
176 an intermediate layer, as previously described [27]. As a control experiment, the spring constant
177 of the NOM-coated AFM probes was measured and compared to those of the silica colloidal
178 probes, where no significant difference was observed. These results indicate no impact of the
179 NOM coating on the nanomechanical properties of the cantilevers. A minimum of 10 force
180 profiles were recorded for every NOM sample at 1, 10, and 100 mM NaCl-containing solutions.
181 The forces recorded were normalized by the radius of the colloidal probe (F/R), presented in
182 units of mN/m, and modeled by Classic and Extended Derjaguin-Landau-Verwey-Overbeek
183 (DLVO) theory (section 2.5). Force profiles were not performed in CaCl_2 -containing solutions

184 because the DLVO theory does not account for specific interactions and complexation between
 185 Ca^{2+} cations and functional groups.

186 **2.5. Modeling of interacting forces between organics and surfaces: Classic and Extended Derjaguin-**
 187 **Landau-Verwey-Overbeek (DLVO) theory.**

188 During approaching regime, interaction force vs. distance curve profiles were modelled
 189 following: a) Decay length, b) Classic DLVO, and c) Extended DLVO theory. Briefly,
 190 experimental Decay length follows an exponential decay described by the equation: $F =$
 191 $F_0 \exp(-\kappa d)$, where F is the interaction force, F_0 is a pre-exponential constant physically
 192 described as the force at contact, κ^{-1} is the interaction force decay length, and d is the separation
 193 distance [34]. Approaching curves were individually analyzed to extract F_0 and κ^{-1} at every
 194 solution condition. Additionally, Classic DLVO theory is described as the sum of van der Waals
 195 (vdW) and electrostatic double-layer interactions (i.e., considering a sphere and an infinite planar
 196 surface) as: $F_{DLVO} = F_{vdW} + F_e$; where A_{123} is the Hamaker constant, r is the radius of the
 197 colloidal AFM probe, d is the separation distance between the AFM colloidal probe and mica
 198 surface, ψ_t and ψ_s are the surface potentials of the NOM-coated AFM colloidal probe and model
 199 mica surface, respectively, κ is the inverse Debye length, k is the Boltzmann constant, e is the
 200 electron charge, T is the absolute temperature, z is the valence, ε is the dielectric constant of the
 201 solution, and ε_0 is the dielectric permittivity of vacuum (Eq. 1-2) [35].

$$202 \quad F_{vdW} = \frac{A_{132}}{6} \left[-\frac{r}{d^2} - \frac{r}{(d+2r)^2} + \frac{2r}{d(d+2r)} \right] \quad (3)$$

$$203 \quad F_e = 4\pi\varepsilon\varepsilon_0(\kappa r) \left(\frac{kT}{ze} \right)^2 \psi_t \psi_s \left[\frac{\exp(-\kappa r d)}{1 + \exp(-\kappa r d)} - \frac{(\psi_t - \psi_s)^2}{2\psi_t \psi_s} * \frac{\exp(-2\kappa r d)}{1 - \exp(-2\kappa r d)} \right] \quad (2)$$

$$204 \quad F_{XDLVO} = F_{DLVO} + F_0 \exp\left(-\frac{h}{\lambda}\right)$$

205 Besides vdW and electrostatic forces, an extended DLVO model considered the contribution of
206 steric repulsive forces as previously described (Eq. 3) [36]. λ is a characteristic Decay length of
207 possible steric nature. All the experimental Force-Distance profiles were modeled using
208 nonlinear regression by OriginPro v.2018, providing a physical description of the influence of
209 electrostatics, vdW, and steric repulsive forces during NOM interactions with surfaces.

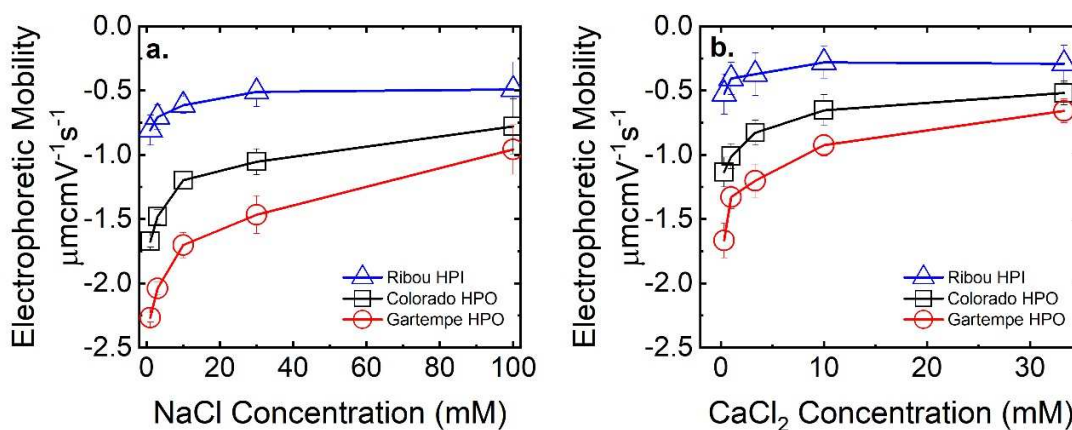
210 ***2.6. Aggregation Kinetics of capped AgNPs in NOM-Containing Electrolyte Solutions***

211 The stability of TA-coated and silica-coated AgNPs was studied by the TR-DLS technique in
212 NOM-containing electrolyte solutions using a ZS ZEN3600 Zetasizer (Malvern, UK) and low
213 volume plastic disposable cuvettes (ZEN112, Malvern, UK). The intensity-weighted
214 hydrodynamic diameter (D_h) of capped AgNPs was calculated by second-order cumulant
215 analysis using Dispersion Technology Software (v5.10, 2008, Malvern, UK) as previously
216 described [37]. The initial hydrodynamic diameter (D_{ho}) of capped AgNPs was measured by
217 diluting the stock suspensions in a 1 mM NaCl solution to a final concentration of 1 ppm and to a
218 final volume of 500 μ L and was used as a baseline for the following aggregation kinetics
219 experiments. During TR-DLS experiments, TA-coated or silica-coated AgNPs were added to the
220 electrolyte solution to a final concentration of 1 ppm and to a final salt concentration of 1, 3, 10,
221 30, 50, and 100 mM NaCl, or 0.33, 1, 3.33, 10, 16.6, and 33 mM $CaCl_2$ (i.e., selected as
222 representative for fresh and brackish water sources), gently shook, and placed in the Zetasizer
223 equipment for immediate measurement. The autocorrelation functions were accumulated for 20
224 s, and the measurements extended over 1 h. Similar to the previous experimental condition,
225 capped AgNPs and NOM were simultaneously added to electrolyte solution to a final
226 concentration of 1 ppm and 10 mg C/L, respectively. The latter condition was selected based on
227 the NOM concentration found in their respective aquifers [38, 39]. The experimental aggregation
228 kinetic rate constant (k_{11}) of capped AgNPs in an electrolyte solution or NOM-containing

229 electrolyte solution was calculated during early stages of aggregation as the initial rate of
 230 increase in the nanoparticles hydrodynamic diameter (D_h) as a function of time (t) (i.e., slope),
 231 up to the point at which D_h reaches the relative hydrodynamic diameter of $1.38D_{h0}$, as described
 232 elsewhere [37]. The experimental aggregation kinetic rate constant (k_{11}) of capped AgNPs
 233 provided fundamental information of diffusion-limited and reaction-limited regimes (i.e.,
 234 favorable/unfavorable aggregation) as a function of solution conditions.

235 3. Results and Discussion

236 3.1. Electrophoretic mobility of NOM fractions



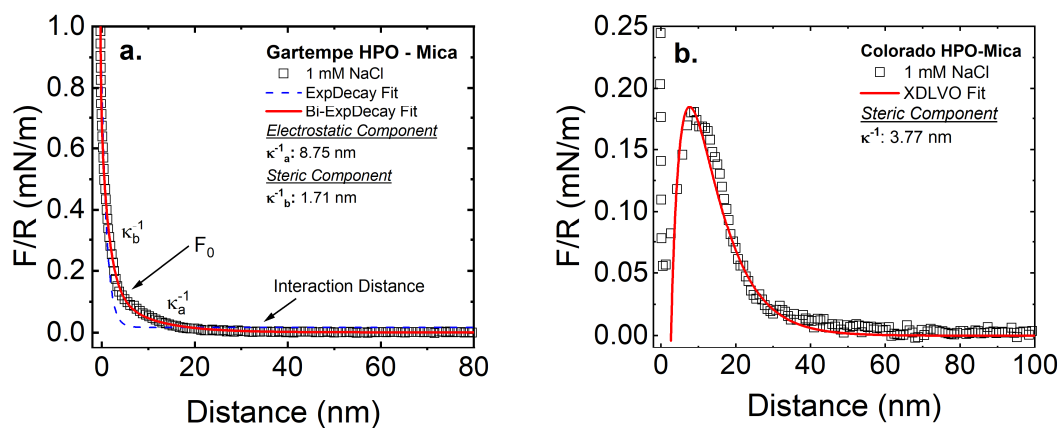
237
 238 **Figure 1:** EPM of Ribou-HPI, Colorado-HPO, and Gartempe-HPO in a) 1, 3, 10, 30, and 100
 239 mM NaCl and b) 0.33, 1, 3.33, 10, and 33.3 mM CaCl_2 solutions

240 The EPM of the three organic fractions were negative throughout the entire NaCl and CaCl_2
 241 concentration range tested (Figure 1). In NaCl solutions, the EPM of the three isolates became
 242 less negatively-charged with increasing ionic strength (Figure 1a). Nevertheless, the magnitude
 243 of the negative charge of these isolates followed the order of Gartempe HPO > Colorado HPO >
 244 Ribou HPI. These differences in EPM would be fundamental during interactions with the capped
 245 AgNPs and ions in solution and can be explained by the physicochemical characteristics of the
 246 NOM fractions, summarized as follows (Table S1-S2) [20, 27, 30, 31]. Briefly, Gartempe-HPO

247 (i.e., hydrophobic acids) was found rich in carboxylic acids (i.e., deprotonated at neutral pH
248 conditions due to their low pKa [40], and main contributor to the charge of the NOM) and
249 aromatic ring structures, while signals of carbohydrates and proteins were almost absent in ¹³C-
250 NMR and FT-IR spectra. Also, this isolate presented a predominance of fulvic acid structures,
251 typical of surface water humic substances. Conversely, Ribou HPI (i.e., hydrophilic colloids)
252 showed a weak presence of aromatic ring structures and carboxyl groups (i.e., explaining its low
253 EPM). Interestingly, a high organic nitrogen content, a large presence of proteins,
254 polysaccharides, and aminosugars were observed. Carbohydrates (i.e., aliphatic structures and
255 alcoholic functional groups) constituted a major fraction in this isolate (analysis is provided in
256 the SI section). Alcoholic groups would not contribute to the charge of the molecule due to its
257 high pKa [40]; however, they play a role during acid-base interactions. Additionally, through
258 contact angle measurements and the calculation of interfacial free energy of interaction with
259 water (ΔG_{121}), previous studies have reported the higher hydrophilicity of -OH than of -COOH
260 groups [41, 42]. These characteristics conferred Ribou-HPI of a strong hydrophilic character.
261 Colorado-HPO also showed a predominance of fulvic acid structures, however, derived from
262 terpenoids. Although significant, the phenolic, aromatic, and carboxyl group contents were lower
263 than that of Gartempe-HPO. Remarkably, this fraction showed abundant polysaccharides
264 moieties and high alcoholic group content [30, 31]. Similarly, the negative charge of the three
265 organic fractions decreased with increasing CaCl₂ concentration in solution (Figure 1b) and also
266 followed the order of Gartempe HPO > Colorado HPO > Ribou HPI. However, the magnitude of
267 the negative charge of the organics in CaCl₂ solutions was lower than those in NaCl solutions
268 throughout the whole range of ionic strength. Previous studies have observed similar trends [20,
269 32, 43]. Ca²⁺ would exert an influence on the surface properties of the organics, possibly through

270 cation complexation with deprotonated carboxyl groups [44]. This latter observation would
 271 indicate the importance of the characteristics of these organic fractions during interactions with
 272 other surfaces and colloids in solution (e.g., capped AgNPs). The abovementioned characteristics
 273 (e.g., aromaticity, aliphaticity, carbohydrate/protein content, carboxyl, alcoholic, methyl
 274 functional groups) defined the hydrophobic and hydrophilic nature of the NOM fractions; and
 275 thus, would exert an impact during interactions with ions and the capping agents of AgNPs.

276 **3.2. Interfacial interactions between NOM and mica surface**



277
 278 **Figure 2:** Representative force vs. distance curves during approaching regime between the mica
 279 surface and a) Gartempe HPO or b) Colorado HPO-coated colloidal probe. The forces were
 280 normalized by the radius of the colloidal probe (F/R) and presented in units of mN/m.

281 NOM changes the surface properties of the capping agents upon adsorption and, thus, influences
 282 the interfacial interactions of the capped nanoparticles with other components of aquatic systems
 283 (e.g., colloids, ions). Therefore, AFM in contact mode was used to study the contributions of van
 284 der Waals, electrostatics, and steric mechanisms of every NOM isolate during interfacial
 285 interactions. The force vs. distance curves during approaching regime between the mica surface
 286 and the three organic isolates showed different profiles. Briefly, during Gartempe HPO
 287 approaching to the mica surface, long-ranged repulsive forces were initially recorded at an

288 interaction distance of approximately 30 nm in 1 mM NaCl-containing solution (Figure 2a).
289 These repulsive forces increased with decreasing interaction distance, following an exponential
290 profile until a linear response of the cantilever (i.e., constant compliance region) and overcoming
291 attractive vdW forces. The magnitude of these repulsive forces decreased with increasing NaCl
292 concentration in solution due to the: a) charge screening and b) compression of polymeric
293 structures of the organic fraction, thus, resulting in decreased inter/intramolecular repulsive
294 forces as previously suggested [45]. Regardless of the ionic strength of the solution, no jump-
295 into-contact effect was observed between Gartempe HPO and the mica surface in all the force
296 curves recorded. A jump-into-contact occurs when the spring constant of the cantilever is
297 exceeded by the gradient of the attractive forces between the surface and colloidal probe during
298 approaching regime [46]. An exponential decay fit could not successfully describe the profile of
299 the approaching curves (Figure 2a); thus, indicating additional interactive mechanisms between
300 Gartempe HPO and mica besides electrostatics. Nevertheless, the force profile was described by
301 a bi-exponential decay fit (Figure 2a), indicating two regions of different interacting
302 mechanisms. Additional details regarding decay and Debye length calculations are provided in
303 the SI section. Previous studies have observed similar trends in the force vs. distance
304 approaching curves between NOM-coated surfaces [33, 47]. Two decay lengths were extracted,
305 where the first decay length would correspond to long-ranged interactions of electrostatic nature,
306 while the second decay length would be assigned to repulsive steric forces caused by the
307 compression of the polymeric structures of Gartempe HPO. Specifically, the magnitude of the
308 decay length of the first region was highly dependent on the solution chemistry and was close to
309 the theoretical Debye length (e.g., 8.87, 4.39, and 2.02 nm vs. 9.84, 3.11, and 0.98 nm for 1, 10,
310 and 100 mM NaCl, respectively) [35]. This latter observation is consistent with the

311 physicochemical characteristics of this organic fraction and its high EPM (Figure 1). Conversely,
312 the decay length of the second region showed lower values and less sensitive to solution
313 conditions (e.g., 1.68, 1.51, and 0.89 nm for 1, 10, and 100 mM NaCl, respectively).

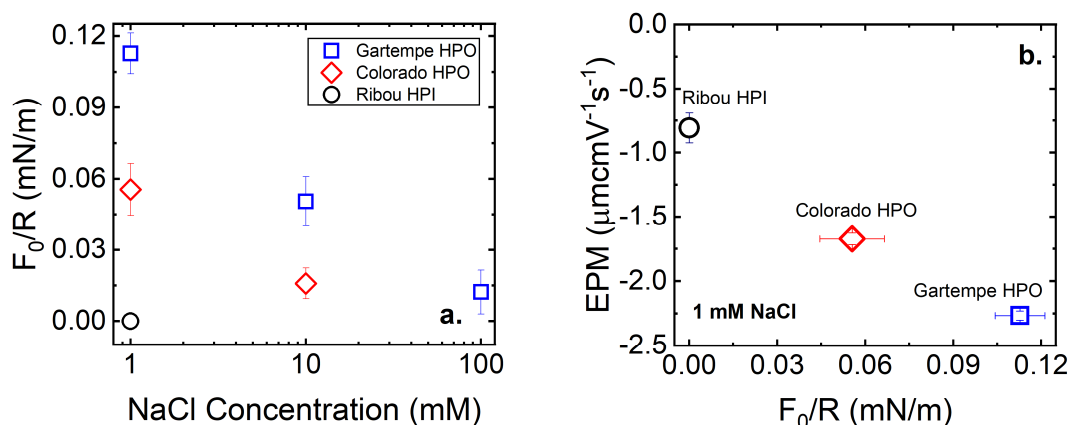
314 Similarly, the force vs. distance curves between Colorado HPO and the mica surface also showed
315 increasing repulsive forces with decreasing interaction distance following a pseudo-exponential
316 decay, possibly of electrostatic and steric nature (Figure 2b). Nevertheless, jump-into-contact
317 events were recorded following the long-ranged repulsive forces, suggesting another type of
318 dominant interacting mechanism at short distances. Jump-into-contact events were observed in
319 every force-curve irrespective of ionic strength in solution. The gradient of the attractive forces
320 inducing jump-into-contact would be caused by a combination of low electrostatic repulsive
321 forces, attractive vdW forces, and acid-base interactions (i.e., hydrogen bonds between hydroxyl
322 groups present in Colorado HPO and electronegative elements in the mica surface), as previously
323 suggested [45, 48]. Specifically, Colorado-HPO showed polysaccharides moieties and alcoholic
324 group content (i.e., absent in Gartempe-HPO); thus, contributing to its affinity towards mica. The
325 magnitude of the decay length corresponding to the long-range electrostatic repulsive forces was
326 also dependent on the solution chemistry and close to the theoretical Debye length (e.g., 8.21 and
327 2.78 for 1 and 10 mM NaCl, respectively). Moreover, the XDLVO model assisted in elucidating
328 the contribution of the short-range forces of possible steric nature (Eq. 3). The characteristic
329 Decay length (λ) extracted at 1 mM NaCl (i.e., 3.77 nm) was higher than that of Gartempe HPO
330 (Figure 2b), suggesting steric repulsive forces as an additional mechanism interacting between
331 Colorado NOM and the mica surface. Additional details regarding XDLVO calculations are
332 provided in the SI section. On the other hand, jump-into-contact events have been recognized as
333 unstable regimes that prevent the accurate measurement of attractive forces and induce

334 misinterpretations regarding zero-distances [34]; thus, difficulting the modeling and physical
335 description of attractive short-range forces. Thus, the current study did not further study this
336 phenomenon.

337 Conversely, the force vs. distance curves between Ribou HPI and mica surface showed no
338 repulsive forces even at low ionic strength (1 mM NaCl), where the screening of charges is not
339 significant (Figure S2). This low electrostatic repulsion (i.e., low electrostatic repulsive forces
340 below the detection limit of the AFM) would be explained by the physicochemical
341 characteristics of this fraction and also clearly evidenced by its low EPM (Figure 1). Specifically,
342 this fraction is characterized by the weakest presence of carboxyl groups among the three NOM
343 selected. Nonetheless, polysaccharides, aminosugars, aliphatic structures, and alcoholic
344 functional groups constituted a major fraction contributing to the hydrophilic character of Ribou
345 HPI (analysis is provided in the SI section), and thus, to the high affinity to the super hydrophilic
346 mica surface. As a consequence, jump-into-contact events were recorded at all solution
347 conditions, possibly caused by a combination of attractive vdW forces and strong acid-base
348 interactions between the dominant alcoholic groups in the structure of Ribou HPI and
349 electronegative elements in the mica surface [48].

350 In summary, the combination of high electrostatic charge, steric forces induced by its polymeric
351 nature, and its high aromatic/phenolic carbon content would cause the high repulsion and lack of
352 jump-into contact events between Gartempe-HPO and the highly electronegative and hydrophilic
353 mica. On the other hand, the lower charge, aromatic carbon, and phenolic content, in addition to
354 abundant polysaccharide moieties and alcoholic groups, would induce short-range attractive
355 forces of acid-base nature that caused jump-into-contact events between Colorado-HPO and

356 mica. Conversely, the hydrophilic nature and considerably low charge of Ribou HPI would
357 induce jump-into contact events and the lowest repulsion forces to mica (i.e., high affinity).

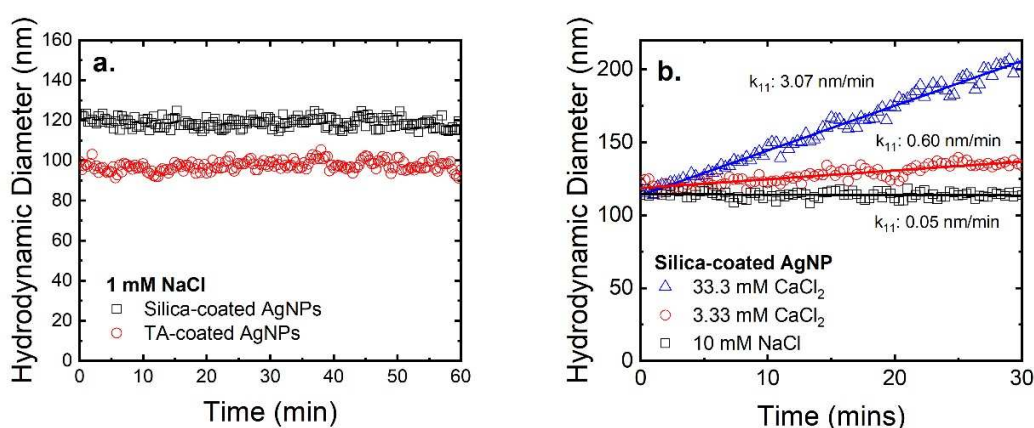


358
359 **Figure 3:** a) Repulsive electrostatic forces between NOM isolates and mica surface in NaCl
360 solutions of different ionic strengths. b) Zeta potential of NOM isolates vs. repulsive electrostatic
361 forces between NOM isolates and mica surface in a 1 mM NaCl solution. The forces were
362 normalized by the radius of the colloidal probe (F/R) and presented in units of mN/m.

363 The force at contact (F_0) was extracted from the fitting of the electrostatic component (i.e., long-
364 range interactions) of the approaching curve of Gartempe HPO, Colorado HPO, and Ribou HPI,
365 as previously described [33, 47], and plotted against the NaCl concentration (Figure 3a). This
366 force at contact (F_0) would represent the approximate maximum electrostatic repulsive force
367 recorded between the NOM-coated AFM probe and the mica surface before contact. Due to well-
368 known uncertainties (e.g., heterogeneity in the thickness of the NOM-coating layer, the
369 molecular weight of the NOM structures, molecular arrangements within the coating layer),
370 determining the exact point of contact has been previously reported as challenging [49]. Due to
371 its extremely low magnitude, the F_0 value of Ribou HPI at 1 mM NaCl was set as zero nN (i.e.,
372 no repulsive force was detected prior jump-into-contact events). The magnitudes of F_0 for the
373 three organic fractions followed the order of: Gartempe HPO > Colorado HPO > Ribou HPI (i.e.,
374 consistent with their respective physicochemical characteristics) and sharply decreased with

375 increasing ionic strength in solution, indicating charge screening (Figure 3a). Additionally, a
 376 strong correlation between the EPM and F_0 values of the three organics was observed (Figure
 377 3b); thus, indicating the importance of the physicochemical characteristics of these organics
 378 during long-range electrostatic interactions. Electrostatic forces play a key role in the energy
 379 barriers between surfaces during interactions in solution [35]. Therefore, understanding the
 380 electrostatic and steric forces generated by the selected NOM fractions would assist in predicting
 381 the interfacial interactions between NOM and capped AgNPs in electrolyte solutions, ultimately
 382 leading to colloidal stability or aggregation.

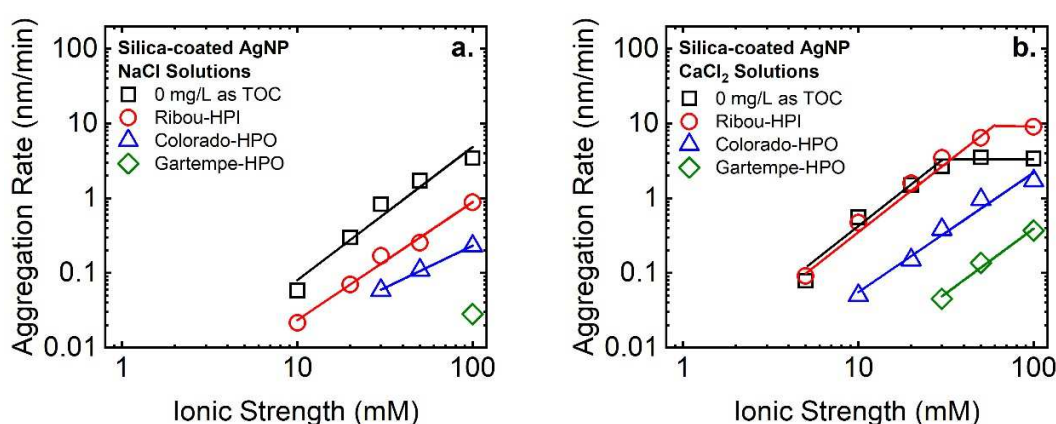
383 **3.3. Aggregation kinetics of tannic acid-coated and silica-coated AgNPs in NOM-containing**
 384 **electrolyte solutions**



385
 386 **Figure 4:** Aggregation kinetic of: a) Silica-coated and TA-coated AgNPs in 1 mM NaCl, and b)
 387 silica-coated AgNPs in 10 mM NaCl, 3.33 mM CaCl₂, and 33.3 mM CaCl₂.

388 The hydrodynamic diameter (D_h) of both silica-coated and TA-coated AgNPs was measured for
 389 60 min in a 1 mM NaCl solution to determine their stability in solution and initial hydrodynamic
 390 diameters (D_{ho}) for further aggregation kinetics experiments (Figure 4a). Both types of
 391 nanoparticles showed high stability and a D_{ho} of 118.9 ± 2.5 nm and 97.3 ± 2.5 nm for silica-coated
 392 and TA-coated AgNPs, respectively. TA is a molecule (isoelectric point < 2 and ~ 1.7 kDa)

393 commonly used for the stabilization of silver and gold nanoparticles in solution. In contrast,
394 silica (isoelectric point~3) is a versatile coating option for nanomedicine, biodiagnostic,
395 photothermal applications, and color. Also, silica preserves the optical properties and provides
396 good salt stability to silver and gold nanoparticles. At environmentally relevant pH, both silica
397 and TA acquire a negative charge, which would be fundamental during interactions with
398 organics in solution.



399
400 **Figure 5:** Aggregation kinetics of silica-coated AgNPs in a) NaCl and b) CaCl₂ solutions, in the
401 absence and presence (10 mg C/L) of NOM
402 In the presence of increased NaCl concentration, the silica-coated AgNPs showed decreasing
403 stability in solution due to simple charge screening (Figure S4). The aggregation rate (k_{11}) of
404 silica-coated AgNPs increased from 0.05 to 0.30, 0.83, 1.72, and 3.43 nm/min for 10, 20, 30, 50
405 and 100 mM NaCl-containing solutions, respectively (Figure 4b and 5a, Table S3). No clear
406 critical coagulation concentration (CCC) was observed at high ionic strength (IS). CCC is
407 defined at the limit concentration between reaction-limited and diffusion-limited regimes [37].
408 On the other hand, the aggregation rates of silica-coated AgNPs in CaCl₂-containing solutions
409 were slightly higher than those in NaCl, indicating the influence of cation bridging (i.e., specific
410 interactions) on the destabilization of these nanoparticles (Figure 4b and 5b). The EPM of silica-

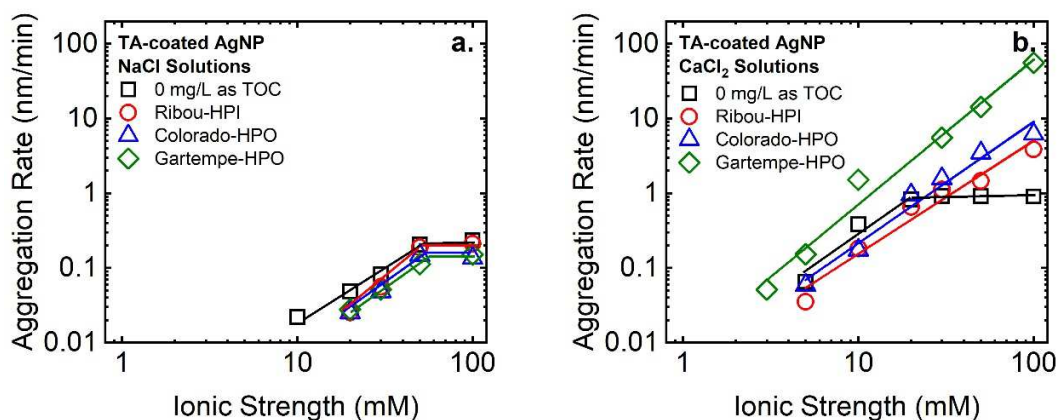
411 coated AgNPs in CaCl₂ was significantly lower than those in NaCl solution in the whole IS
412 tested; thus, confirming the latter observation. Specifically, at 1.66 mM CaCl₂ (5 mM IS) the k_{11}
413 was 0.08 nm/min and increased to 0.60, 1.50, 2.67, 3.52, and 3.07 nm/min at 3.33, 6.66, 10,
414 16.66, and 33.3 mM CaCl₂ (10, 20, 30, 50, and 100 mM IS), respectively (Table S3). Thus, CCC
415 was recorded at approximately 13.3 mM CaCl₂ (40 mM IS). Previous studies have observed bare
416 AgNPs to readily aggregate at low salt concentrations in solution (i.e., CCC < 10 mM NaCl, and
417 CCC < 1 mM CaCl₂); thus, mainly attributed to the low electrostatic stabilization of the bare Ag
418 surface [22, 50]. Therefore, the silica coating provided colloidal electrostatic stabilization to the
419 AgNPs.

420 Remarkably, in the presence of NOM-containing NaCl solution, the silica-coated AgNPs showed
421 enhanced stabilization. Nevertheless, the level of stabilization (k_{11}) highly depended on the
422 characteristics of the NOM. Briefly, the aggregation of silica-coated AgNPs in the presence of
423 Gartempe HPO was solely detected at 100 mM NaCl with a k_{11} of 0.03 nm/min, which was two
424 order of magnitude lower than the corresponding k_{11} (3.43 nm/min) in the absence of NOM
425 (Figure 5a). Colorado HPO also proved efficient in stabilizing silica-coated AgNPs at high ionic
426 strength; however, their aggregation rates were approximately 1.5 orders of magnitude lower
427 than those in the absence of NOM (Figure 5a). Additionally, no CCC was observed. On the other
428 hand, the presence of the hydrophilic fraction (Ribou HPI) also induced stability to the silica-
429 coated AgNPs, resulting in a 5-fold decrease of k_{11} compared to those in the absence of NOM
430 (Figure 5a). These results clearly indicate the adsorption of the organic fractions on the silica
431 capping (i.e., change in surface properties) and subsequent stabilization of the nanoparticles
432 through electrostatic and steric mechanisms. Interestingly, the level of stabilization of
433 nanoparticles in solution followed the same trend as observed during the AFM-EPM experiments

434 (Figures 2 and 3), where Gartempe HPO and Ribou HPI showed the highest and lowest repulsive
435 forces, respectively. Specifically, Gartempe HPO adsorbed on silica-coated AgNPs would
436 generate the highest energy barriers against successful collisions (i.e., and subsequent
437 aggregation) through a combination of electrostatic and steric repulsive forces. These energy
438 barriers would decrease with increasing NaCl concentration in solution due to simple charge
439 screening (Na^+) and compression of polymeric structures. Conversely, among the three NOM
440 selected, Ribou HPI showed the lowest and highest presence of carboxyl and alcoholic
441 functional, respectively. Based on these characteristics, low electrostatic repulsive forces (i.e.,
442 inducing low energy barriers) and attractive acid-base interactions (occurring at short separation
443 distances) would play a key role during the aggregation between silica-coated AgNPs in Ribou
444 HPI-containing solutions. In brief, the most hydrophobic NOM fraction (Gartempe-HPO)
445 provided the highest stability to silica-coated AgNPs in NaCl solutions based on electrosteric
446 mechanisms. Remarkably, this stability decreased with increasing hydrophilicity of the NOM
447 fraction due to lower electrostatic repulsion and attractive acid-base interactions occurring at
448 short separation distances.

449 Remarkably, Ca^{2+} cations radically impacted the stability of silica-coated AgNPs in NOM-
450 containing solutions (Figure 5b and S3b). The aggregation behavior was also highly dependent
451 on the characteristics of the organic fractions. Briefly, aggregation of silica-coated AgNPs in
452 Gartempe HPO-containing solutions was initially observed at 10 mM CaCl_2 (k_{11} : 0.05 nm/min)
453 and increased with increasing CaCl_2 concentration (k_{11} : 0.37 nm/min at 33.3 mM CaCl_2);
454 however, no CCC was observed. Similarly, the aggregation of silica-coated AgNPs in Colorado
455 HPO-containing solutions was initially recorded at low divalent cation concentrations (3.3 mM
456 CaCl_2) and showed a 7-fold increase in aggregation rates compared to those in NaCl.

457 Interestingly, at low CaCl_2 (i.e., 1.66, 3.33, and 10 mM CaCl_2), the aggregation rates of silica-
 458 coated AgNPs in Ribou HPI-containing solutions were similar to those in the absence of NOM.
 459 Nevertheless, at higher CaCl_2 concentrations (i.e., 16.6 and 33.3 mM CaCl_2), the presence of
 460 Ribou HPI induced enhanced aggregation in silica-coated AgNPs (Figure 5b). These results
 461 clearly indicated cation bridging as a dominant interaction mechanism between the deprotonated
 462 carboxyl groups in the organics adsorbed on the silica-coated AgNPs, and between organics and
 463 silica-coated AgNPs; thus, inducing aggregation. In a previous study, AFM was used to measure
 464 the adhesion forces between citrate-coated AgNPs and NOM in NaCl vs. CaCl_2 -containing
 465 solutions, providing evidence of cation bridging mechanism [20]. Although it was not possible to
 466 confirm the full or partial NOM coating on the silica surface, the adsorption of these organic
 467 fractions changed the surface properties of the silica-coated AgNPs and was key for the stability
 468 and aggregation behavior of these nanoparticles in solution.



469
 470 **Figure 6:** Aggregation kinetics of TA-coated AgNPs in a) NaCl and b) CaCl_2 solutions, in the
 471 absence and presence (10 mg C/L) of NOM

472 A low aggregation of TA-coated AgNPs (k_{11} : 0.02 nm/min) was observed in 10 mM NaCl. The
 473 aggregation rates increased with increasing NaCl in the solution until CCC was observed at
 474 approximately 50 mM NaCl (k_{11} : 0.20 nm/min) (Figure 6a and S3b). Remarkably the

475 aggregation rates of TA-coated AgNPs were approximately one order of magnitude lower than
476 those of silica-coated AgNPs under the same Na^+ concentration. The surface characteristics of
477 both types of nanoparticles played a crucial role in their aggregation behavior. Although the
478 EPM of both capped AgNPs were similar at low IS, the EPM of silica-coated AgNPs decreased
479 more with increasing IS than that of TA-coated AgNPs. This latter result indicates that ions exert
480 a higher impact on the surface of silica-coated AgNPs. Also, the silica coating is a hard and
481 smooth surface following classic DLVO interaction forces [35]. On the other hand, TA is an
482 organic molecule providing additional steric repulsive mechanisms due to its polymeric nature
483 [33, 47]. However, in CaCl_2 solutions of low concentrations (e.g., 3.33 to 10 mM CaCl_2), the
484 aggregation rates of TA-coated AgNPs were slightly one order of magnitude higher than those in
485 NaCl (Figure 6b and S3b). Also, a CCC was recorded at approximately 6.66 mM CaCl_2 (i.e., 20
486 mM ionic strength). These results indicate the impact of divalent cations through cation bridging
487 between deprotonated carboxyl groups in the TA structure; thus, inducing enhanced aggregation
488 and overcoming the steric mechanism provided by the polymeric structure of TA.[44]

489 Unlike silica-coated AgNPs, the presence of organics in solution did not radically change the
490 aggregation behavior of TA-coated AgNPs in NaCl -containing solutions (Figure 6a).
491 Specifically, the aggregation rates of TA-coated AgNPs slightly decreased in Gartempe HPO,
492 Colorado HPO, or Ribou HPI, and the CCC in these three conditions was still recorded at
493 approximately 50 mM NaCl . This latter observation indicates the low interactions between TA-
494 coated AgNPs and NOM in Na^+ -containing solutions. Nevertheless, Ca^{2+} cations in solution
495 induced enhanced aggregation through cation bridging between deprotonated carboxyl groups on
496 the structure of both organic fractions and TA-coated AgNPs (Figure 6b and S3b). The changes
497 recorded in the aggregation rates were correlated to the characteristics of the organics in solution.

498 The magnitude of k_{11} across the tested CaCl_2 range followed the order of: Gartempe HPO >
499 Colorado HPO > Ribou HPI. Based on their structures, the two HPO fractions (i.e., highly acidic
500 in nature) present more carboxyl groups than the Ribou HPI fraction (i.e., where aliphatic
501 structures and alcoholic groups are dominant in its structure). Additionally, the presence of
502 carboxyl groups in the structure of organics has been commonly correlated to their EPM or zeta
503 potential [20, 27]. Therefore, the high aggregation rates of TA-coated AgNPs in Gartempe HPO-
504 containing solutions, exceeding those of Colorado HPO and Ribou HPI, would be caused by a
505 higher content of deprotonated carboxyl group interacting through Ca^{2+} cations inner-sphere
506 complexation with TA and Gartempe HPO molecules themselves [44]. Besides, no CCC was
507 observed in the aggregation behavior of TA-coated AgNPs for the three organics tested,
508 indicating reaction-limited aggregation even at higher CaCl_2 concentrations. These results clearly
509 indicate the electrostatic and steric stabilization of AgNPs by the TA coating and the strong
510 interactions between NOM and TA in Ca^{2+} -containing solutions, which ultimately impact the
511 stability of the coated-nanoparticles.

512 **4. Conclusions**

513 The results presented in the current study introduce profound environmental implications. Silica
514 and tannic acid are widely-used capping agents providing different surface properties to AgNPs
515 as a function of their industrial target. Nevertheless, the release of these coated nanoparticles in
516 the environment poses multiple threads to diverse aquatic ecosystems and human health. The
517 experimental conditions in the current study tested the homoaggregation of capped nanoparticles
518 under different solution chemistries and the presence of NOM. In natural aquifers, the
519 aggregation of capped nanoparticles would be induced by colloids through heteroaggregation.
520 Nevertheless, understanding the interactions between the capping agents and ubiquitous

521 components of the environment (e.g., NOM of different properties, cations, IS) is also crucial for
522 understanding and predicting the fate and transport of capped-AgNPs in natural aquatic systems.
523 The current results show that the physicochemical characteristics of the capping agents play a
524 crucial role in the interfacial interactions with NOM and ions in solution. The hard and smooth
525 surface of silica provided some stability in solution to the AgNPs (i.e., following classic DLVO
526 mechanisms). However, this silica surface also showed strong interactions with both humic and
527 non-humic organics in Na⁺-containing solutions, ultimately deriving in NOM adsorption onto
528 silica (i.e., change in surface properties), and enhanced stability. Humic NOMs provided more
529 stability to the silica-coated AgNPs than its non-humic counterpart, mainly due to stronger
530 electro-steric repulsive forces. Conversely, the polymeric TA provided higher stability to the
531 AgNPs than silica coating and also showed weak interactions with NOM in the presence of Na⁺
532 in solution. Ca²⁺ induced the aggregation of TA-coated and silica-coated AgNPs in NOM-
533 containing solutions through specific interactions (i.e., cation bridging). However, humic NOM
534 induced faster aggregation of both types of nanoparticles in Ca²⁺-containing solutions due to its
535 higher content of deprotonated carboxyl groups (i.e., cation bridging). These results indicate that:
536 i) tannic acid as a capping agent, and ii) the adsorption of NOM onto the silica coating induce
537 high stability in AgNPs. Due to the ubiquitous and dominant presence of humics in natural
538 waters, the latter scenario would be highly possible. Remarkably, the aggregation rates of capped
539 AgNPs would be correlated to the NOM concentration in the aquifers. In aquifers of high ionic
540 strength and hardness (e.g., estuaries), the aggregation of these capped AgNPs would be
541 expected, and their transport would be limited. Contrariwise, in freshwater (i.e., low ionic
542 strength and presence of NOM), these capped nanoparticles would travel long distances.
543 Nevertheless, different species would be preferentially affected by stable or aggregated AgNPs.

544 For instance, planktonic organisms in suspension would be more exposed to colloiddally stable
545 AgNPs, while benthic organisms living in sediments would be exposed to aggregated/sedimented
546 AgNPs. The latter scenario is also fundamental during the risk assessment of AgNPs in natural
547 aquatic systems.

548 **Acknowledgments**

549 The authors are grateful to Dr. Denise Mitrano for providing the Ag nanoparticle samples.

550 **References**

- 551 [1] N. Singh, B. Manshian, G.J.S. Jenkins, S.M. Griffiths, P.M. Williams, T.G.G. Maffei, C.J. Wright, S.H.
552 Doak, *NanoGenotoxicology: The DNA damaging potential of engineered nanomaterials*, *Biomaterials*, 30
553 (2009) 3891-3914.
- 554 [2] M. Ahamed, M.S. AlSalhi, M.K.J. Siddiqui, Silver nanoparticle applications and human health, *Clin.*
555 *Chim. Acta*, 411 (2010) 1841-1848.
- 556 [3] S.A. Blaser, M. Scheringer, M. MacLeod, K. Hungerbühler, Estimation of cumulative aquatic exposure
557 and risk due to silver: Contribution of nano-functionalized plastics and textiles, *Sci. Total Environ.*, 390
558 (2008) 396-409.
- 559 [4] J. Gao, K. Powers, Y. Wang, H. Zhou, S.M. Roberts, B.M. Moudgil, B. Koopman, D.S. Barber, Influence
560 of Suwannee River humic acid on particle properties and toxicity of silver nanoparticles, *Chemosphere*,
561 89 (2012) 96-101.
- 562 [5] C. Gil-Allué, K. Schirmer, A. Tlili, M.O. Gessner, R. Behra, Silver Nanoparticle Effects on Stream
563 Periphyton During Short-Term Exposures, *Environ. Sci. Technol.*, 49 (2015) 1165-1172.
- 564 [6] B.P. Colman, B. Espinasse, C.J. Richardson, C.W. Matson, G.V. Lowry, D.E. Hunt, M.R. Wiesner, E.S.
565 Bernhardt, Emerging Contaminant or an Old Toxin in Disguise? Silver Nanoparticle Impacts on
566 Ecosystems, *Environ. Sci. Technol.*, 48 (2014) 5229-5236.
- 567 [7] C. Levard, E.M. Hotze, B.P. Colman, A.L. Dale, L. Truong, X.Y. Yang, A.J. Bone, G.E. Brown, R.L.
568 Tanguay, R.T. Di Giulio, E.S. Bernhardt, J.N. Meyer, M.R. Wiesner, G.V. Lowry, Sulfidation of Silver
569 Nanoparticles: Natural Antidote to Their Toxicity, *Environ. Sci. Technol.*, 47 (2013) 13440-13448.
- 570 [8] K.L. Chen, M. Elimelech, Aggregation and deposition kinetics of fullerene (C-60) nanoparticles,
571 *Langmuir*, 22 (2006) 10994-11001.
- 572 [9] T. Cosgrove, *Colloid Science: Principles, Methods and Applications*, Wiley, 2010.
- 573 [10] T. Phenrat, N. Saleh, K. Sirk, H.-J. Kim, R.D. Tilton, G.V. Lowry, Stabilization of aqueous nanoscale
574 zerovalent iron dispersions by anionic polyelectrolytes: adsorbed anionic polyelectrolyte layer properties
575 and their effect on aggregation and sedimentation, *J Nanopart Res*, 10 (2008) 795-814.
- 576 [11] E.M. Hotze, T. Phenrat, G.V. Lowry, Nanoparticle aggregation: challenges to understanding
577 transport and reactivity in the environment, *J. Environ. Qual.*, 39 (2010) 1909-1924.
- 578 [12] A.M.E. Badawy, T.P. Luxton, R.G. Silva, K.G. Scheckel, M.T. Suidan, T.M. Tolaymat, Impact of
579 Environmental Conditions (pH, Ionic Strength, and Electrolyte Type) on the Surface Charge and
580 Aggregation of Silver Nanoparticles Suspensions, *Environ. Sci. Technol.*, 44 (2010) 1260-1266.
- 581 [13] B.J.R. Thio, M.O. Montes, M.A. Mahmoud, D.-W. Lee, D. Zhou, A.A. Keller, Mobility of Capped Silver
582 Nanoparticles under Environmentally Relevant Conditions, *Environ. Sci. Technol.*, 46 (2011) 6985-6991.

583 [14] M. Tejamaya, I. Römer, R.C. Merrifield, J.R. Lead, Stability of Citrate, PVP, and PEG Coated Silver
584 Nanoparticles in Ecotoxicology Media, *Environ. Sci. Technol.*, 46 (2012) 7011-7017.

585 [15] Y. Cao, R. Zheng, X. Ji, H. Liu, R. Xie, W. Yang, Syntheses and characterization of nearly
586 monodispersed, size-tunable silver nanoparticles over a wide size range of 7–200 nm by tannic acid
587 reduction, *Langmuir*, 30 (2014) 3876-3882.

588 [16] H. Choi, J.-P. Lee, S.-J. Ko, J.-W. Jung, H. Park, S. Yoo, O. Park, J.-R. Jeong, S. Park, J.Y. Kim,
589 Multipositional Silica-Coated Silver Nanoparticles for High-Performance Polymer Solar Cells, *Nano*
590 *Letters*, 13 (2013) 2204-2208.

591 [17] S. Liu, Z. Zhang, M. Han, Gram-Scale Synthesis and Biofunctionalization of Silica-Coated Silver
592 Nanoparticles for Fast Colorimetric DNA Detection, *Analytical Chemistry*, 77 (2005) 2595-2600.

593 [18] S.K. Sivaraman, I. Elango, S. Kumar, V. Santhanam, A green protocol for room temperature synthesis
594 of silver nanoparticles in seconds, *Current Science (00113891)*, 97 (2009).

595 [19] S.A. Cumberland, J.R. Lead, Particle size distributions of silver nanoparticles at environmentally
596 relevant conditions, *J. Chromatogr. A*, 1216 (2009) 9099-9105.

597 [20] L. Gutierrez, C. Aubry, M. Cornejo, J.-P. Croue, Citrate-Coated Silver Nanoparticles Interactions with
598 Effluent Organic Matter: Influence of Capping Agent and Solution Conditions, *Langmuir*, 31 (2015) 8865-
599 8872.

600 [21] M. Delay, T. Dolt, A. Woellhaf, R. Sembritzki, F.H. Frimmel, Interactions and stability of silver
601 nanoparticles in the aqueous phase: Influence of natural organic matter (NOM) and ionic strength, *J.*
602 *Chromatogr. A*, 1218 (2011) 4206-4212.

603 [22] X. Li, J.J. Lenhart, H.W. Walker, Dissolution-Accompanied Aggregation Kinetics of Silver
604 Nanoparticles, *Langmuir*, 26 (2010) 16690-16698.

605 [23] S.L. Chinnapongse, R.I. MacCuspie, V.A. Hackley, Persistence of singly dispersed silver nanoparticles
606 in natural freshwaters, synthetic seawater, and simulated estuarine waters, *Sci. Total Environ.*, 409
607 (2011) 2443-2450.

608 [24] K.A. Huynh, K.L. Chen, Aggregation Kinetics of Citrate and Polyvinylpyrrolidone Coated Silver
609 Nanoparticles in Monovalent and Divalent Electrolyte Solutions, *Environ. Sci. Technol.*, 45 (2011) 5564-
610 5571.

611 [25] H.M. Chen, C.F. Hsin, R.-S. Liu, J.-F. Lee, L.-Y. Jang, Synthesis and Characterization of Multi-Pod-
612 Shaped Gold/Silver Nanostructures, *The Journal of Physical Chemistry C*, 111 (2007) 5909-5914.

613 [26] Z. Yi, X. Li, X. Xu, B. Luo, J. Luo, W. Wu, Y. Yi, Y. Tang, Green, effective chemical route for the
614 synthesis of silver nanoplates in tannic acid aqueous solution, *Colloids Surf., A*, 392 (2011) 131-136.

615 [27] C. Aubry, L. Gutierrez, J.P. Croue, Coating of AFM probes with aquatic humic and non-humic NOM
616 to study their adhesion properties, *Water Res.*, 47 (2013) 3109-3119.

617 [28] L. Gutierrez, C. Aubry, R. Valladares Linares, J.-P. Croue, Natural organic matter interactions with
618 polyamide and polysulfone membranes: Formation of conditioning film, *Colloids Surf., A*, 477 (2015) 1-8.

619 [29] J.A. Leenheer, J.-P. Croué, M. Benjamin, V. Korshin Gregory, J. Hwang Cordelia, A. Bruchet, R. Aiken
620 George, Comprehensive Isolation of Natural Organic Matter from Water for Spectral Characterizations
621 and Reactivity Testing, in: *Natural Organic Matter and Disinfection By-Products*, American Chemical
622 Society, 2000, pp. 68-83.

623 [30] C. Hwang, S.W. Kranser, G. Amy, A. Bruchet, J.P. Croue, A. Leenheer Jerry, Polar NOM:
624 Characterization, DBPs, Treatment, AWWA Research Foundation, 2001.

625 [31] J.A. Leenheer, J.P. Croué, Characterizing aquatic dissolved organic matter, *Environ. Sci. Technol.*, 37
626 (2003) 18A-26A.

627 [32] L. Gutierrez, T.H. Nguyen, Interactions between rotavirus and natural organic matter isolates with
628 different physicochemical characteristics, *Langmuir*, 29 (2013) 14460-14468.

- 629 [33] S. Sander, L.M. Mosley, K.A. Hunter, Investigation of Interparticle Forces in Natural Waters: Effects
630 of Adsorbed Humic Acids on Iron Oxide and Alumina Surface Properties, *Environ. Sci. Technol.*, 38 (2004)
631 4791-4796.
- 632 [34] H.J. Butt, B. Cappella, M. Kappl, Force measurements with the atomic force microscope: Technique,
633 interpretation and applications, *Surf. Sci. Rep.*, 59 (2005) 1-152.
- 634 [35] J.N. Israelachvili, *Intermolecular and Surface Forces: Revised Third Edition*, Elsevier Science, 2011.
- 635 [36] L.S. Dorobantu, S. Bhattacharjee, J.M. Foght, M.R. Gray, Analysis of Force Interactions between AFM
636 Tips and Hydrophobic Bacteria Using DLVO Theory, *Langmuir*, 25 (2009) 6968-6976.
- 637 [37] S.E. Mylon, C.I. Rinciog, N. Schmidt, L. Gutierrez, G.C.L. Wong, T.H. Nguyen, Influence of Salts and
638 Natural Organic Matter on the Stability of Bacteriophage MS2, *Langmuir*, 26 (2010) 1035-1042.
- 639 [38] G. Makdissy, J.-P. Croué, G. Amy, H. Buisson, Fouling of a polyethersulfone ultrafiltration membrane
640 by natural organic matter, *Water Science and Technology: Water Supply*, 4 (2004) 205-212.
- 641 [39] F.L. Rosario-Ortiz, S.A. Snyder, I.H. Suffet, Characterization of dissolved organic matter in drinking
642 water sources impacted by multiple tributaries, *Water Res.*, 41 (2007) 4115-4128.
- 643 [40] A.G. Kalinichev, R.J. Kirkpatrick, Molecular dynamics simulation of cationic complexation with
644 natural organic matter, *Eur. J. Soil Sci.*, 58 (2007) 909-917.
- 645 [41] J.A. Brant, K.M. Johnson, A.E. Childress, Characterizing NF and RO membrane surface heterogeneity
646 using chemical force microscopy, *Colloids Surf., A*, 280 (2006) 45-57.
- 647 [42] A.E. Contreras, Z. Steiner, J. Miao, R. Kasher, Q. Li, Studying the Role of Common Membrane Surface
648 Functionalities on Adsorption and Cleaning of Organic Foulants Using QCM-D, *Environ. Sci. Technol.*, 45
649 (2011) 6309-6315.
- 650 [43] L. Gutierrez, T.H. Nguyen, Interactions between Rotavirus and Suwannee River Organic Matter:
651 Aggregation, Deposition, and Adhesion Force Measurement, *Environ. Sci. Technol.*, 46 (2012) 8705-
652 8713.
- 653 [44] A.G. Kalinichev, E. Iskrenova-Tchoukova, W.-Y. Ahn, M.M. Clark, R.J. Kirkpatrick, Effects of Ca²⁺ on
654 supramolecular aggregation of natural organic matter in aqueous solutions: A comparison of molecular
655 modeling approaches, *Geoderma*, 169 (2011) 27-32.
- 656 [45] L. Gutierrez, C. Aubry, L. Dramas, P. Aimar, J.-P. Croue, Characterization of *Skeletonema costatum*
657 intracellular organic matter and study of nanomechanical properties under different solution conditions,
658 *Colloids Surf., A*, 506 (2016) 154-161.
- 659 [46] X. Li, B.E. Logan, Analysis of bacterial adhesion using a gradient force analysis method and colloid
660 probe atomic force microscopy, *Langmuir*, 20 (2004) 8817-8822.
- 661 [47] L.M. Mosley, K.A. Hunter, W.A. Ducker, Forces between Colloid Particles in Natural Waters, *Environ.*
662 *Sci. Technol.*, 37 (2003) 3303-3308.
- 663 [48] H. Yamamura, K. Kimura, T. Okajima, H. Tokumoto, Y. Watanabe, Affinity of functional groups for
664 membrane surfaces: Implications for physically irreversible fouling, *Environ. Sci. Technol.*, 42 (2008)
665 5310-5315.
- 666 [49] T.L. Byrd, J.Y. Walz, Interaction force profiles between *Cryptosporidium parvum* oocysts and silica
667 surfaces, *Environ. Sci. Technol.*, 39 (2005) 9574-9582.
- 668 [50] A.M. El Badawy, K.G. Scheckel, M. Suidan, T. Tolaymat, The impact of stabilization mechanism on
669 the aggregation kinetics of silver nanoparticles, *Sci. Total Environ.*, 429 (2012) 325-331.

670